



Detection of Ionospheric Disturbances Associated with Hazards

By: Mohamed Freeshah

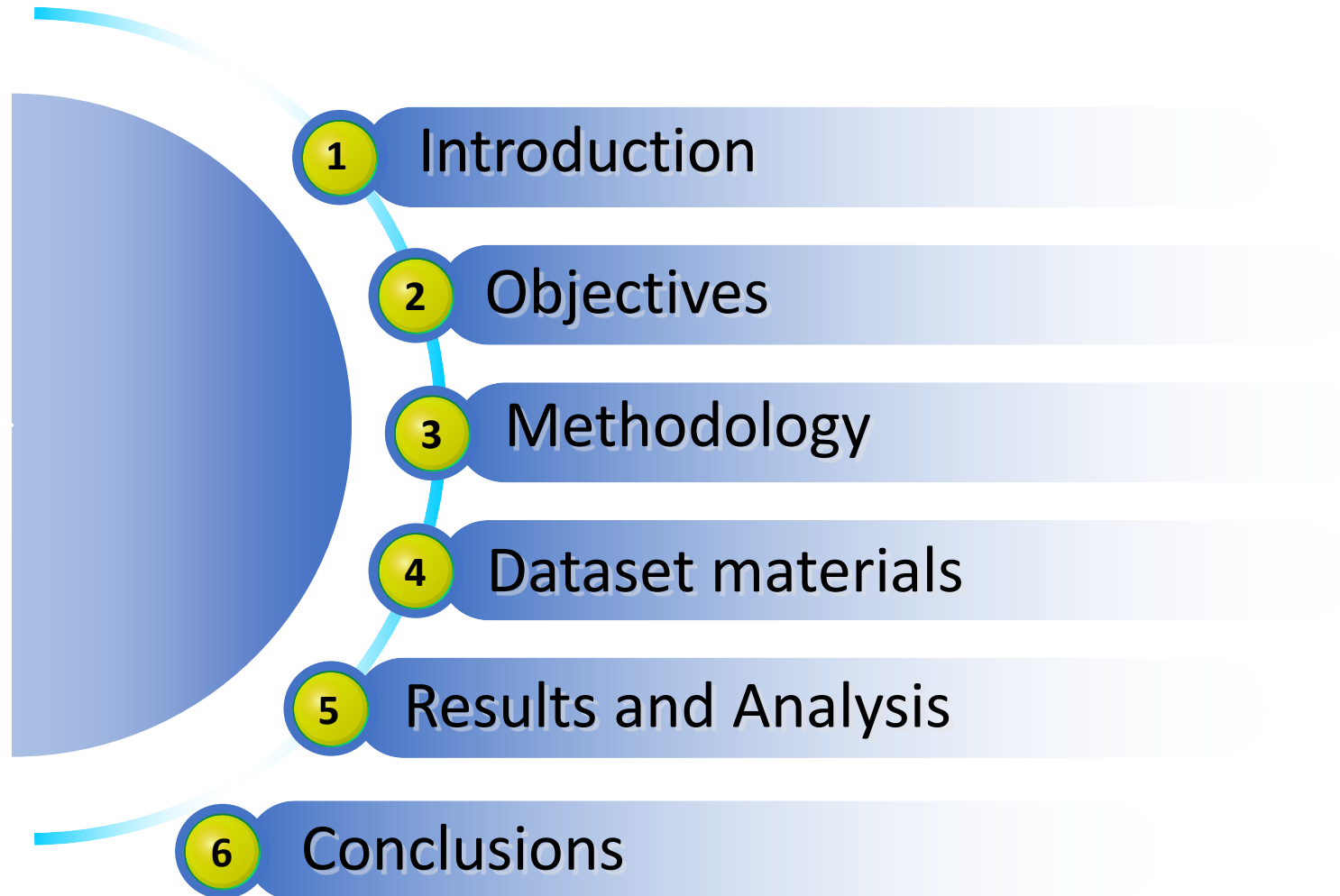
PhD candidate, LIESMARS, Wuhan University

(Mohamedfreeshah@whu.edu.cn)

Supervisor: Prof. Xiaohong Zhang

School of Geodesy and Geomatics, Wuhan University

Contents



Introduction

- Ionosphere is a very important part for navigation and communication signals on our planet.
- Satellites (e.g. GNSS) have to send their signals directly through this turbulent layer.
- Sun caused most of the changes in the ionosphere, but recently even when the sun is relatively quiet. The terrestrial weather patterns and troposphere activities also appear to be involved in the ionospheric fluctuations.

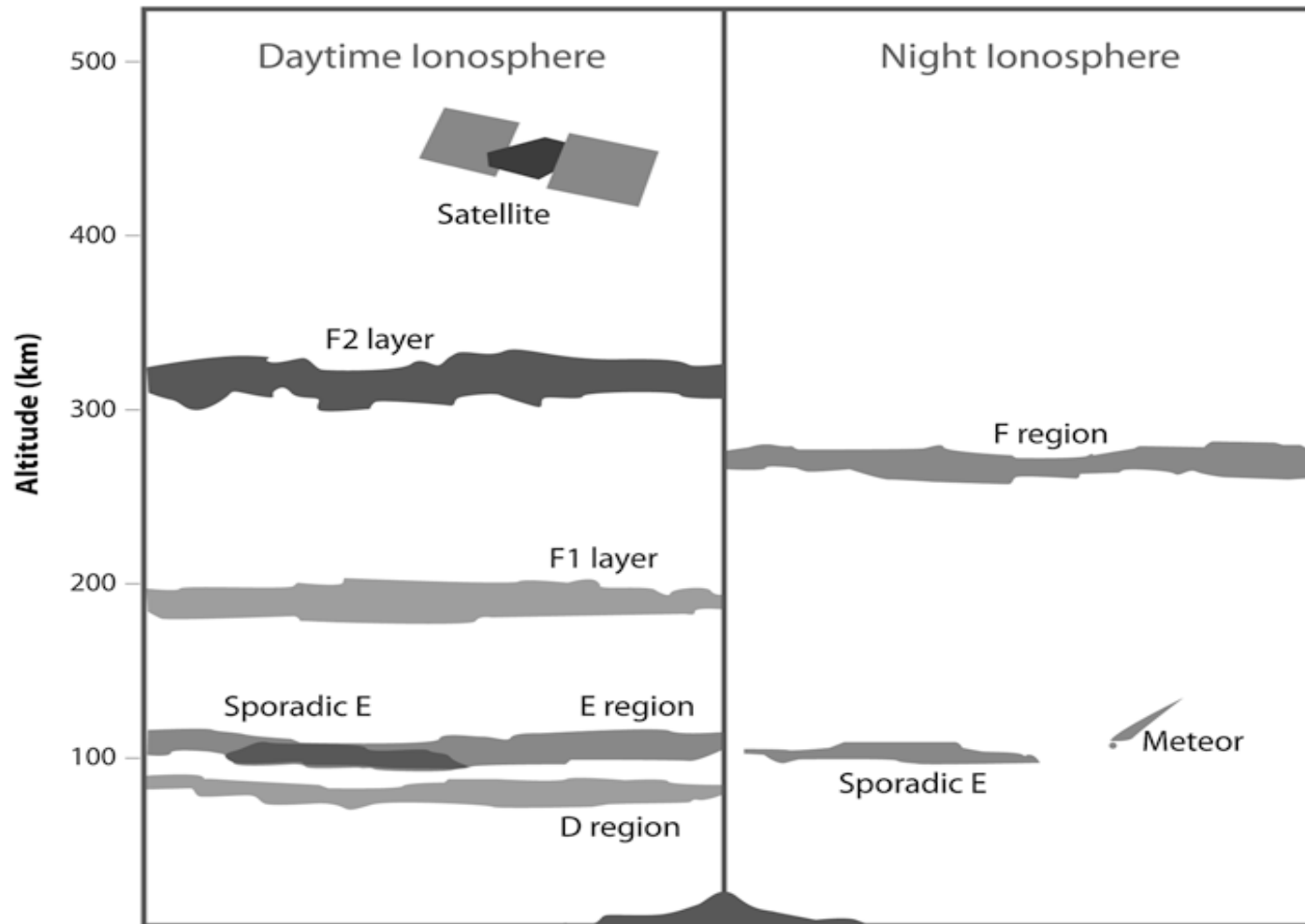
Introduction

- The ionospheric disturbance is caused by the acoustic-gravity waves (AGWs) which generated by hazards (e.g. typhoon, lightning, volcano, etc.)
- Recently, with the rapid developments of GNSS and increase of the number of GNSS receivers, leading to a great breakthrough in the field of space weather monitoring.
- Study the response of the ionosphere to hazards provides a good way to understand the upper atmospheric coupling, where ground or troposphere activities could transfer to the higher atmosphere moreover disturbing it.

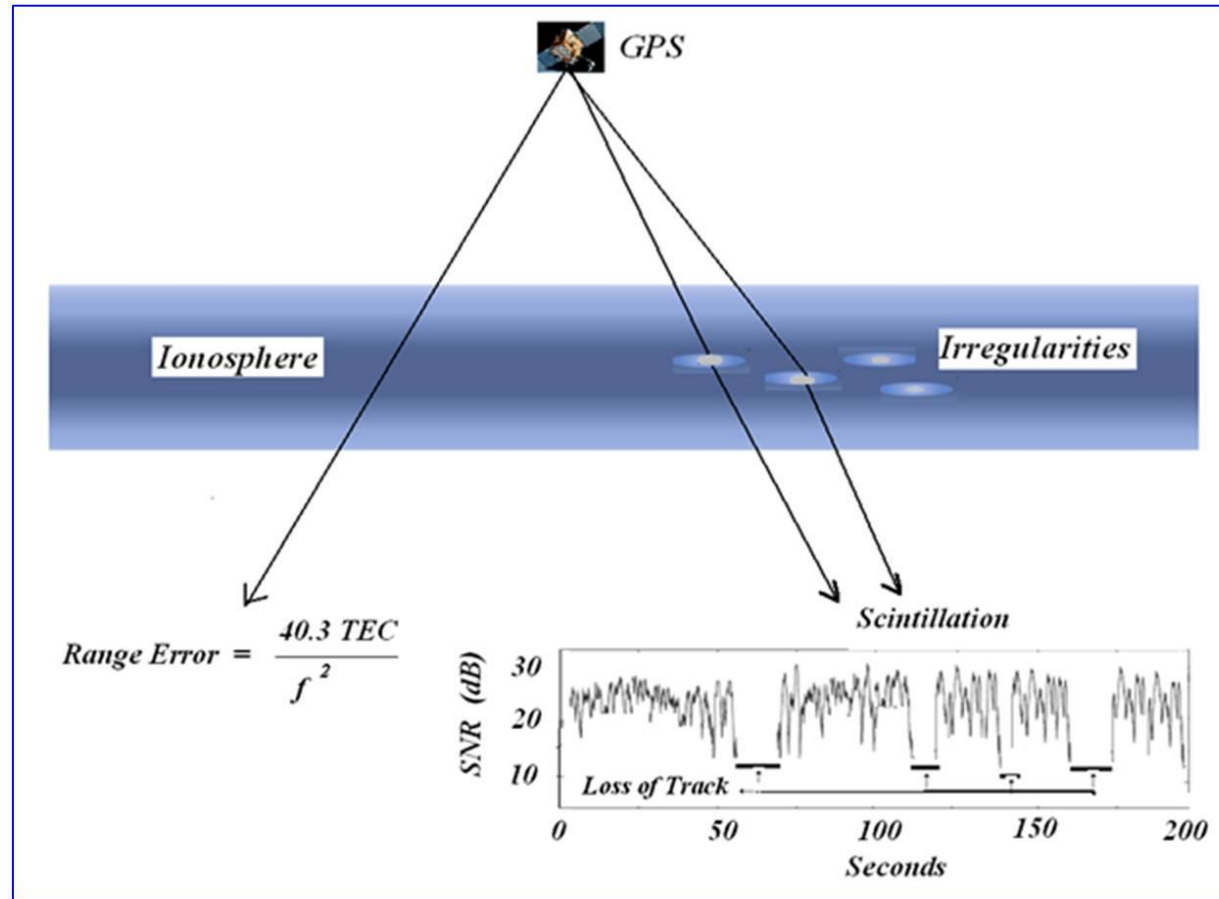
Objectives

- Studying the response of the ionosphere to lightning and Typhoon
- Try to understand the upper atmospheric coupling
- Using multiple Detrending techniques (for removing the effects of accumulated errors from the trendline to display individually the absolute changes in values.)

Ionospheric layers



What happens to the electromagnetic signal?



Methodology

- Ionosphere can effect on the GNSS signals, depending on their frequencies f
- STEC values extended along (LoS) between the receiver and Sat.
- STEC was derived from the dual-frequency GNSS observation:

$$\left\{ \begin{array}{l} P_{r,4}^S = P_{r,1}^S - P_{r,2}^S = \frac{40.3 \times \text{TEC}}{f_1^2} - \frac{40.3 \times \text{TEC}}{f_2^2} + (B_{r,1} - B_{r,2}) + (B_1^S - B_2^S) \\ L_{r,4}^S = L_{r,1}^S - L_{r,2}^S = \frac{40.3 \times \text{TEC}}{f_1^2} - \frac{40.3 \times \text{TEC}}{f_2^2} + (b_{r,1} - b_{r,2}) + (b_1^S - b_2^S) - (N_1 - N_2) \end{array} \right. \quad (1)$$

Where S and r indicate satellite and receiver, TEC is the STEC along LoS; L and P are the carrier phase and pseudorange measurements; f_1 and f_2 are the frequencies of the carrier phases of L_1 and L_2

B^S and B_r are the satellite and receiver hardware delay of the pseudorange code,
 b^S and b_r are the satellite and receiver hardware delay of carrier phase, N is carrier-phase ambiguity.

Methodology

- ionospheric observations can be derived directly from both pseudorange code or carrier phase measurement
- pseudorange measurement contains much noise than that of carrier phase
- precision of the carrier phase is more accurate than that of the pseudorange, but presents the additional problem of biased by unknown ambiguities
- Therefore, the so-called “leveling carrier to code” algorithms

$$L_{I,arc} = L_{Larc} - (L_{Larc} - P_I)_{arc} = TEC + b_r + b^S + (\epsilon_p)_{arc} + \epsilon_L, \quad (2)$$

Where L_{Larc} is the ionospheric observable of carrier-phase ‘leveled’ to the code-delay one, b_r and b^S are the same as Eq. (1), ϵ_p and ϵ_L are the noise and multi-path for the code-delay measurements and for the carrier-phase ionospheric observations

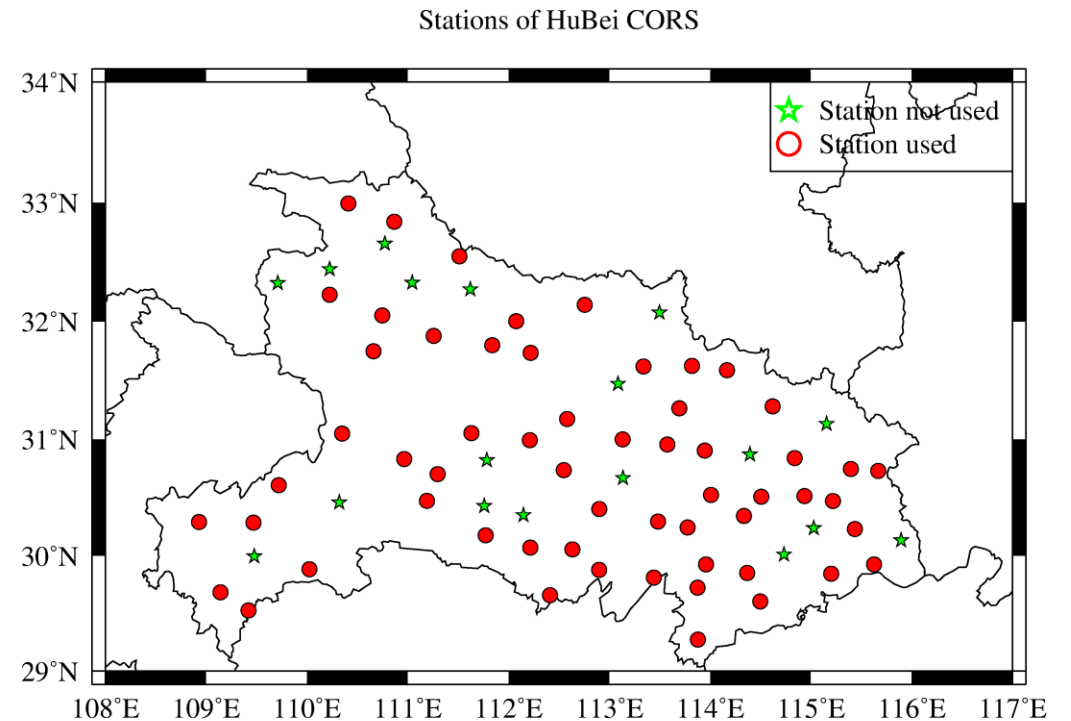
Dataset materials

- F10.7, the solar radiation
- Dst, Kp indices for geomagnetic activity
- GNSS Networks (IGS, CORS,...)
- Hazard information and properties

1st case study “A Strong Thunderstorm over Wuhan City”

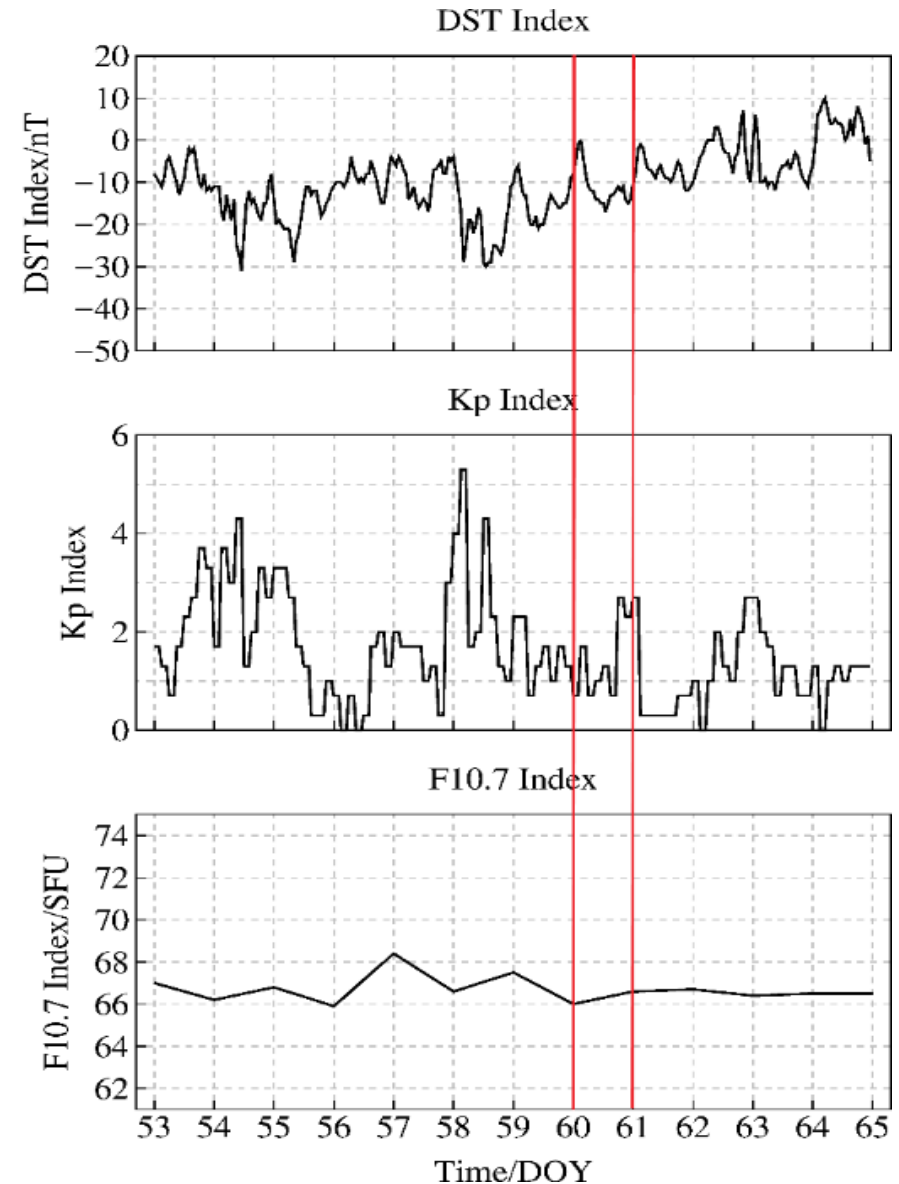
- According to Wuhan Meteorological Observatory, the lightning warning classified as yellow signal besides their strong thunderstorm occurred at 09:00 UT on 2nd March 2018.

- Data sets: Hubei CORS GNSS network



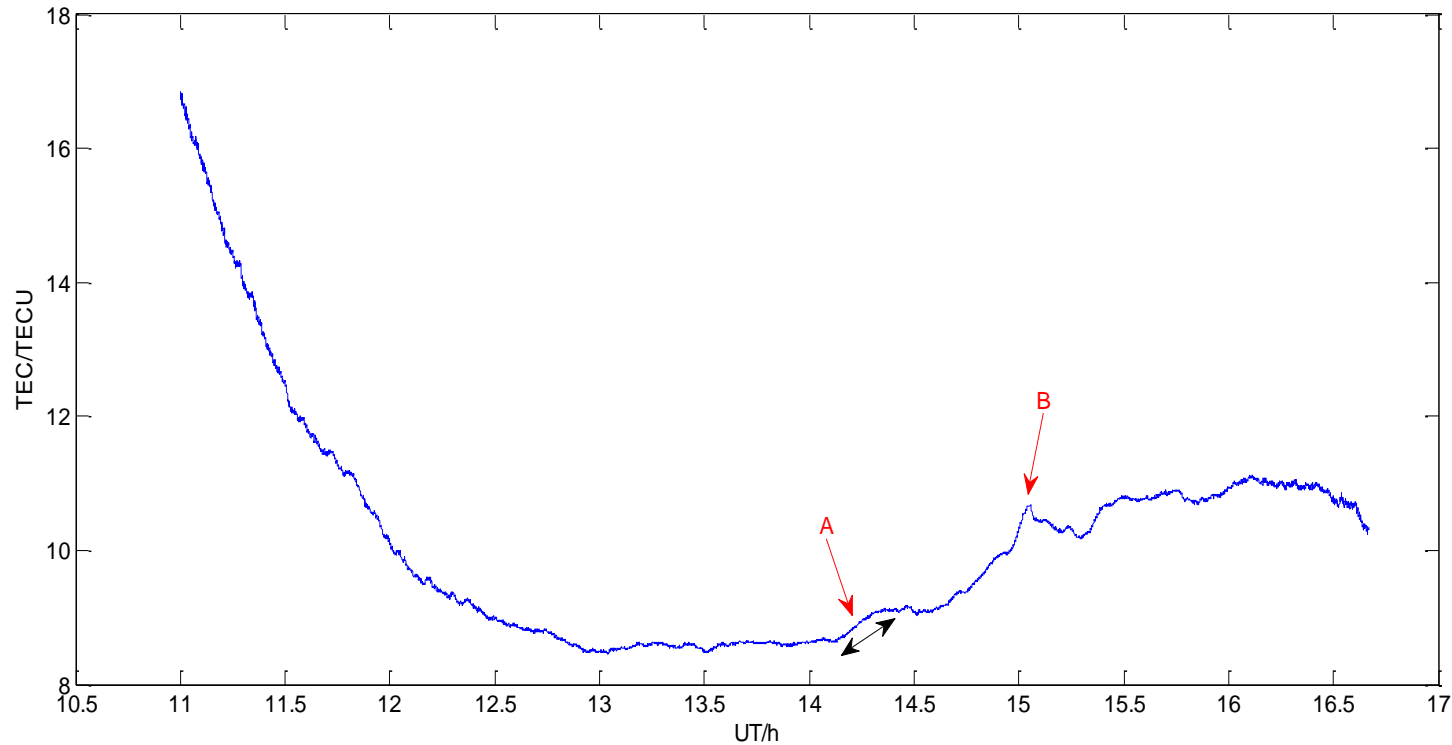
Results and analysis

- Except for Doy54, 58, the geomagnetic conditions are quiet with $Dst < -35\text{nT}$, and $Kp \leq 4$.
- The solar radiation is in a stable state, F10.7 index variation, within 0.3 and 2.5% of its average value
- no presence of strong geomagnetic activity or solar activity is observed



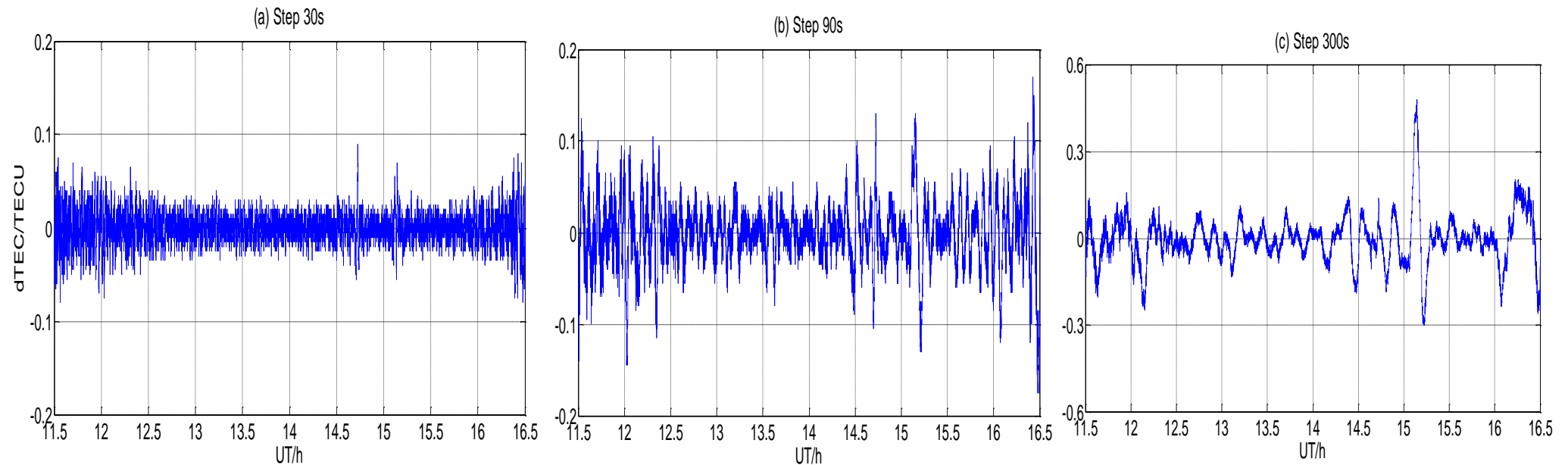
The Disturbance storm-time (Dst) index, geomagnetic Kp index, and solar radio flux F10.7 index during 12 Days (Doy53-Doy65)

Results and analysis



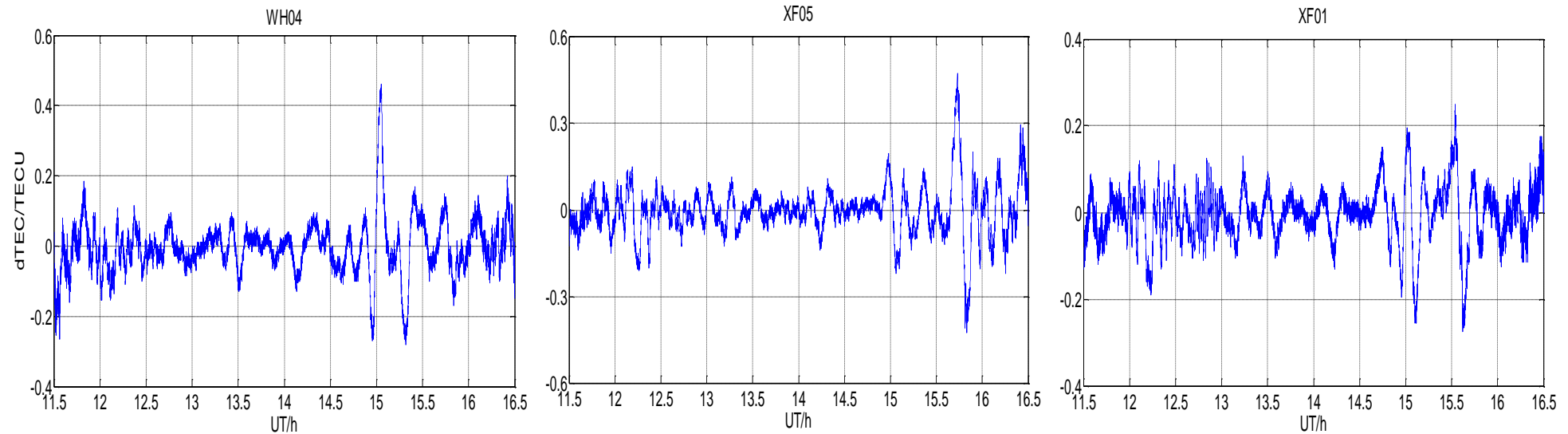
The Ionospheric STEC obtained by GPS observations of the satellite PRN 28 at station WH04. The two arrows indicate the arrival time of ionospheric disturbances.

Results and analysis



Detecting ionospheric disturbances series by **Multi-step numerical difference** technique at station XG04, the order is set to 1, using three different time steps (30, 90 and 300) s, respectively. Panels (a–c) show the results.

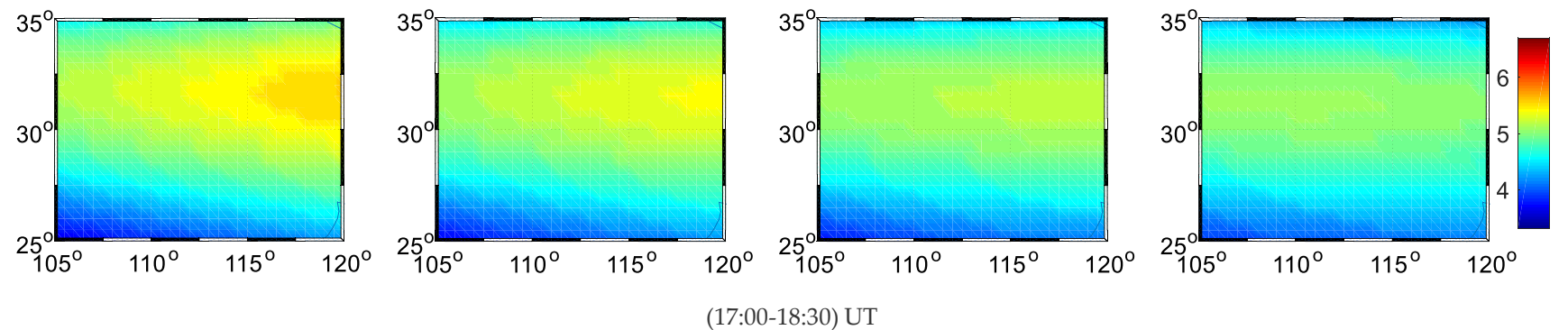
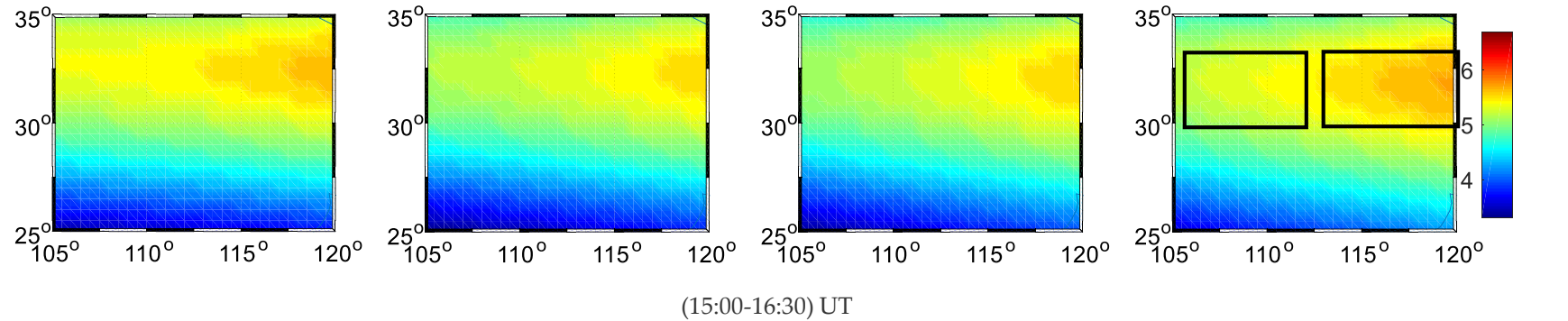
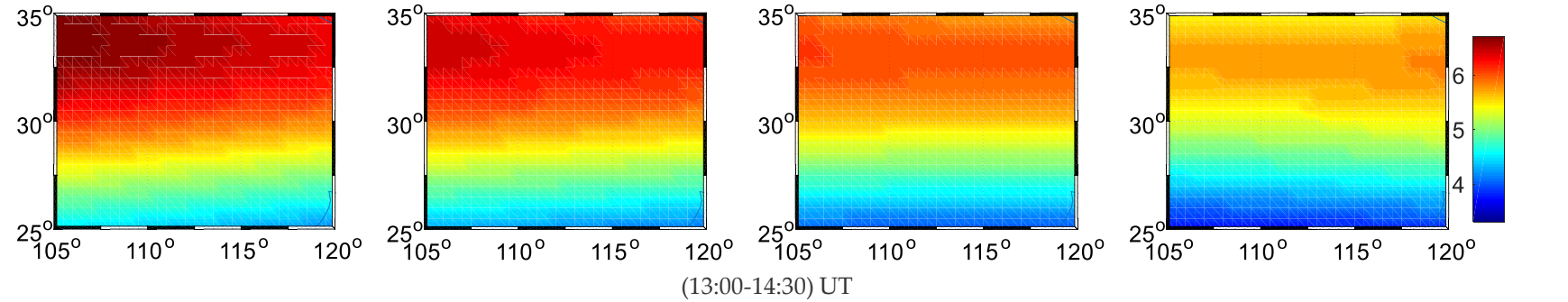
Results and analysis



Detecting ionospheric disturbances series by Multi-step numerical difference technique over other five stations, the order is set to 1, using 300S time step 300 s.

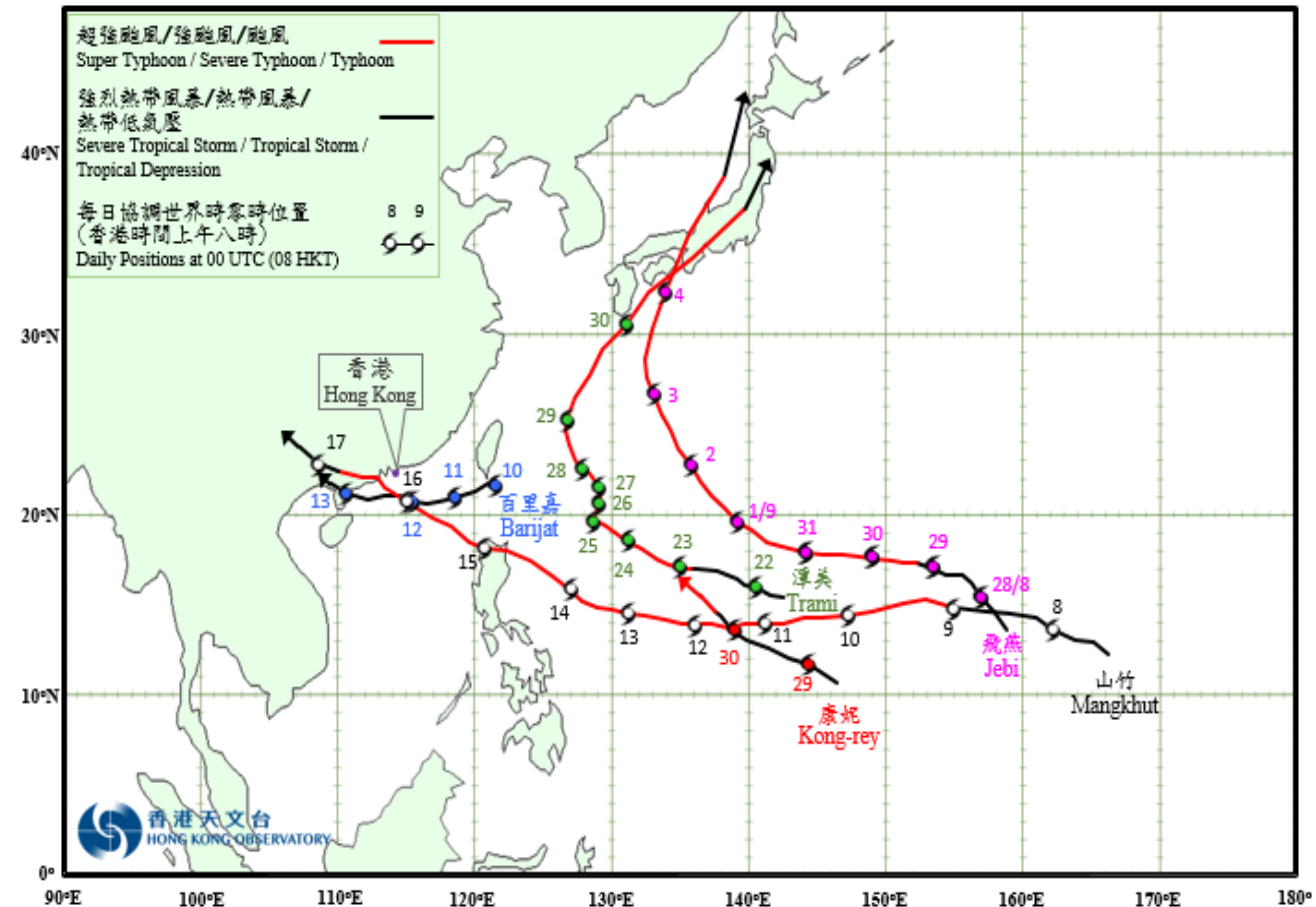
Results and analysis

VTEC maps for Hubei province
obtained from HBCORS every
30 mins.



2nd case study “Mangkhut Tropical Typhoon hits Hong Kong in September 2018”

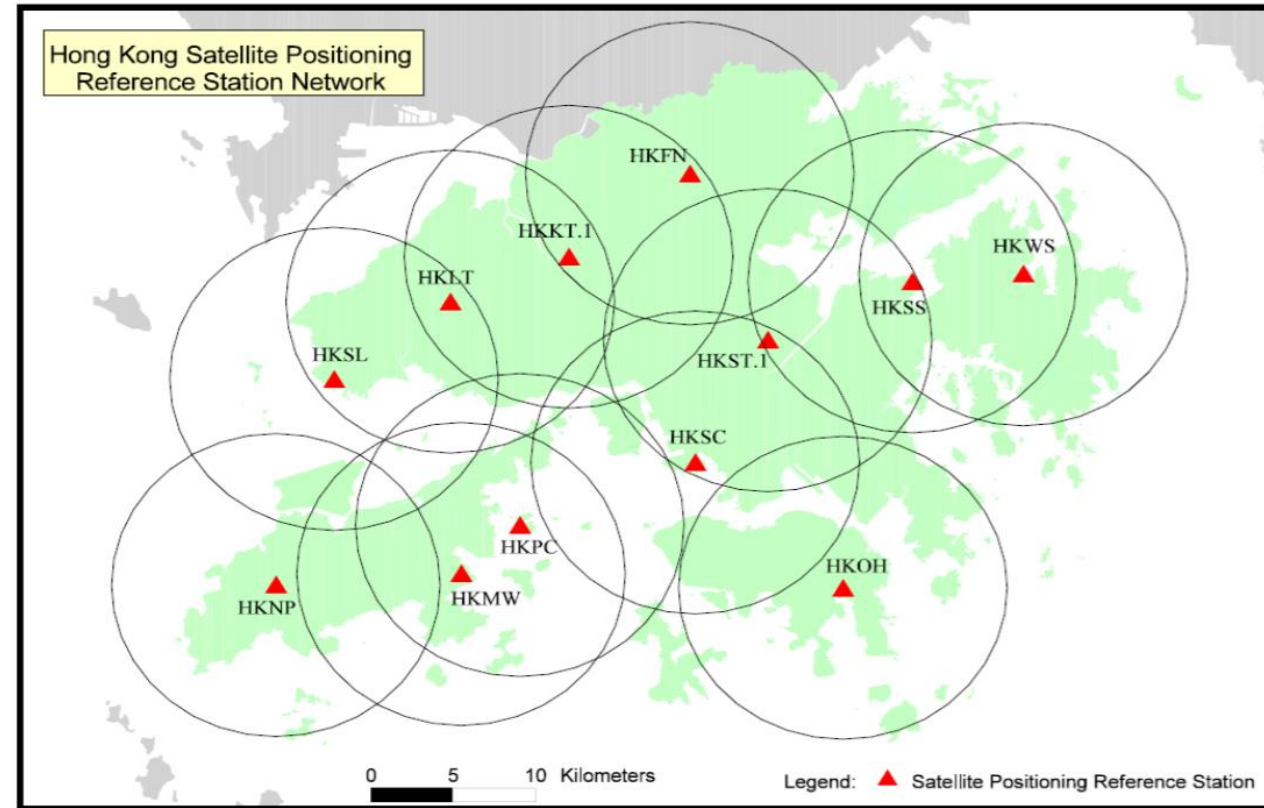
- In September 2018, Mangkhut tropical cyclone warning signals by the Hong Kong Observatory (HKO)



Provisional Tropical Cyclone Tracks in September 2018

2nd case study “Datasets”

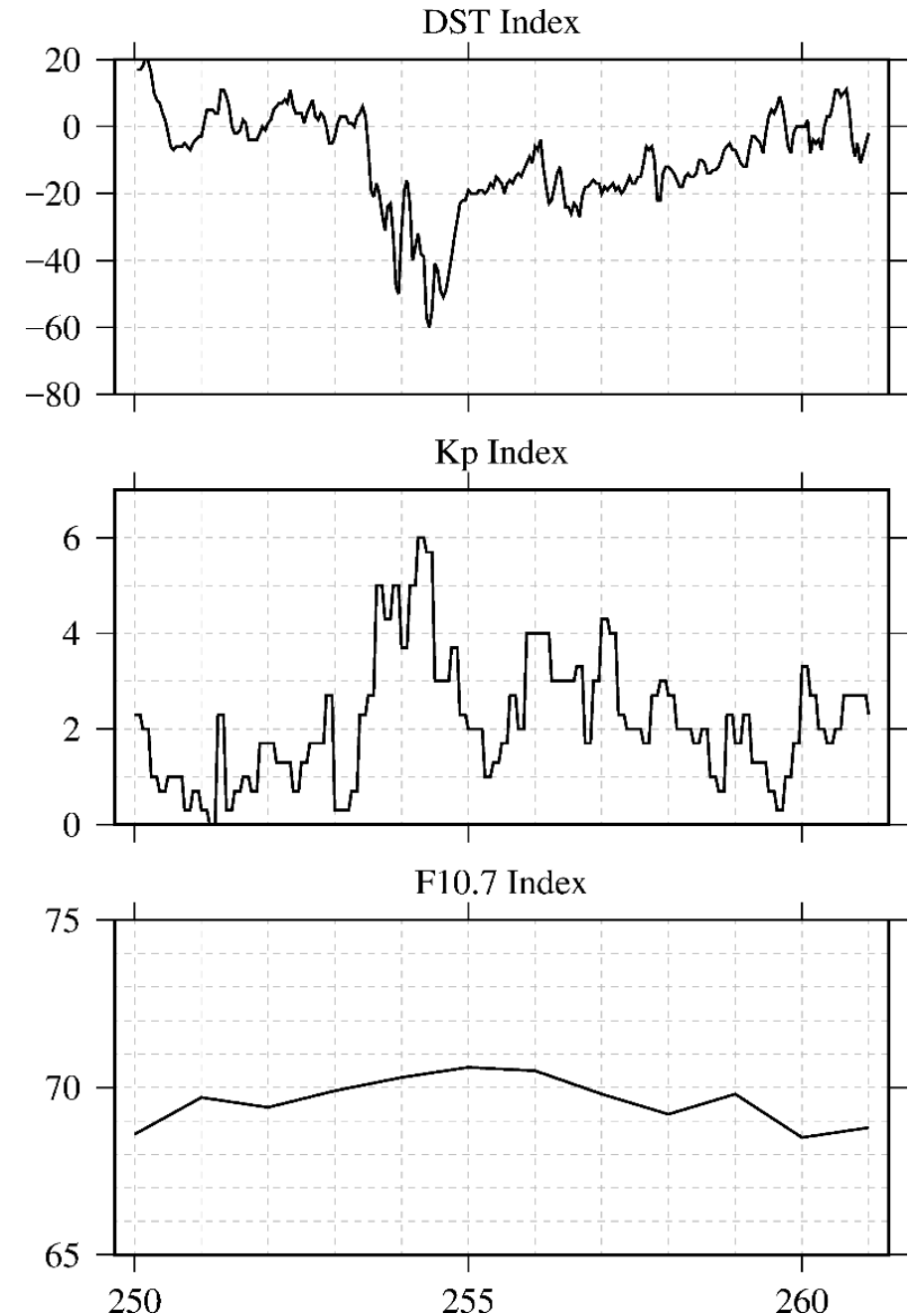
- Data collected from IGS and the Hong Kong Satellite Positioning Reference Station Network (SatRef) in the area around typhoon.
- SatRef consists of 12 Continuously Operating Reference Stations (CORS) evenly set up in Hong Kong.



Distribution of GPS Reference Stations of HK

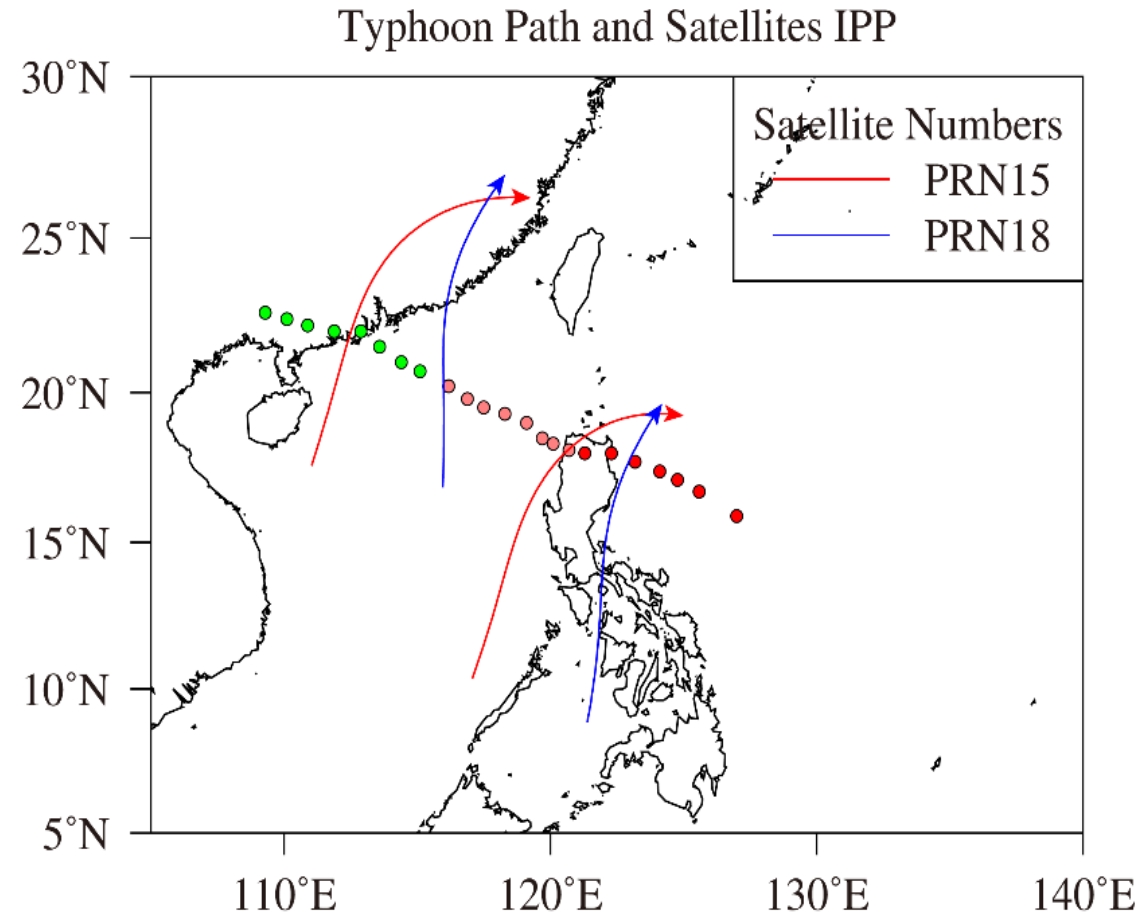
2nd case study “Datasets”

- no presence of strong geomagnetic activity or solar activity was observed
- there is a moderate geomagnetic storm, with $Dst \leq -60\text{nT}$, and $Kp \leq 6$. Except for DOY254, the geomagnetic conditions are quiet.
- F10.7, the solar radiation is in steady state, within 0.1 and 2.1% of its mean value (from DOY250 to DOY260).

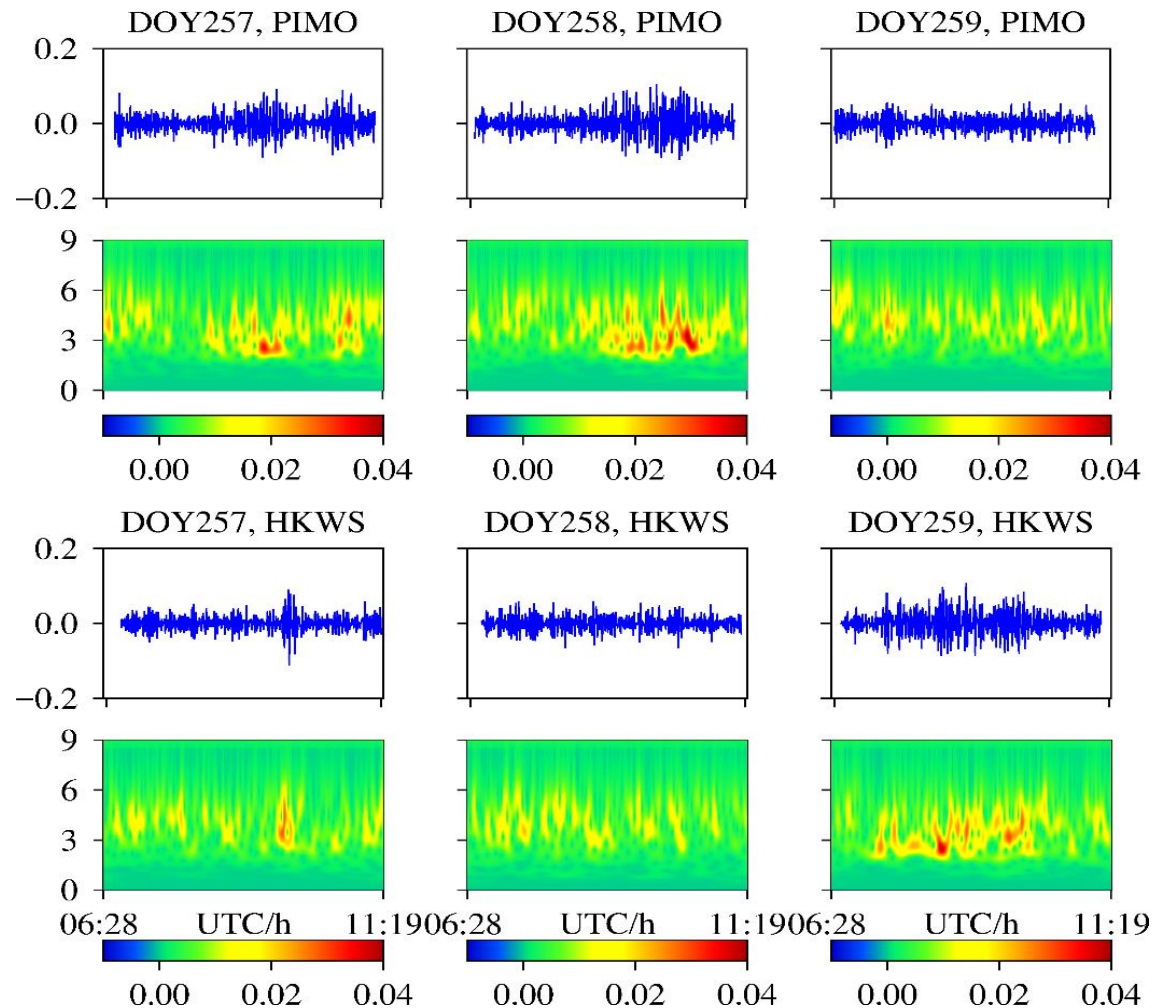


Results and Analysis

- We selected the satellites that can be observed by one station and the whole observation time was in one day.
- PRN 15 and PRN 18 as an example to find ionospheric disturbance caused by the typhoon.
- The IPP of PRN 15 (red lines) and PRN 18 (blue lines) with elevation larger than 30 degrees



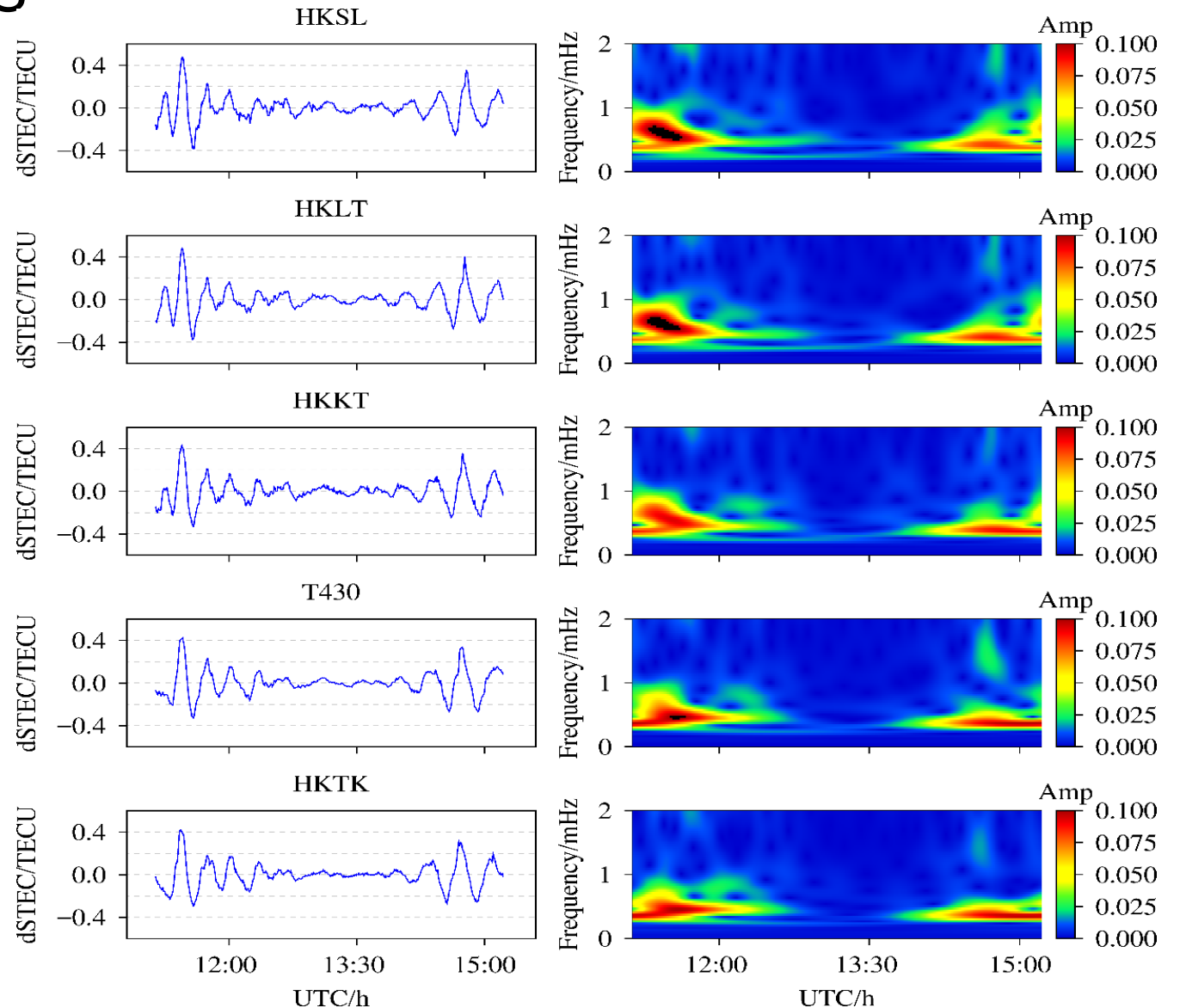
Results and Analysis



De-trend STEC sequences and its spectrum analyze results for PRN 15 observed by PIMO station and HKWS station from DOY 257 to DOY 259.

Results and Analysis

- The de-trend STEC sequences (**Savitzky-Golay smoothing filter**) and its spectrum analyze results for PRN 10 observed by five HK-CORS stations on DOY 259.



CONCLUSIONS

- The AGWs have created by the severe tropical cyclone may transfer to the higher atmosphere.
- Both code-delay and Dual-frequency carrier phase were combined together to derive ionospheric observables represented as the STEC along the LoS.
- We applied de-trend STEC sequences analysis as well as plot spectrum transform to verify the abnormal TEC deviations.
- The comparison results show that when the IPP cross the near center of typhoon, the disturbance can be detected as there are no obvious disturbances on the other days.

Future work

- Going deeply in both case studies to investigate if possible TIDs happened during phenomena
- Try to apply tomography through case studies
- Apply our study at new case studies (Idai cyclone(April, 2019), Total Solar Eclipse (July, 2019), California Earthquake (July, 2019))

Major References

- Freeshah, M.; Zhang, X.; Chen, J. TEC Ionospheric disturbances detection associated with Mangkhut Tropical Cyclone in September 2018 through Hong Kong. The 2019 International Graduate Workshop on Geo-Information, **2019**, Wuhan, China
- Ren, X.; Chen, J.; Li, X.; Zhang, X.; Freeshah, M. Performance evaluation of real-time global ionospheric maps provided by different IGS analysis centers. *GPS Solut.* **2019**, 23: 113. <https://doi.org/10.1007/s10291-019-0904-5>
- Salem, M.A.; Liu, N.; Rassoul, H.K. Effects of small thundercloud electrostatic fields on the ionospheric density profile. *Geophys. Res. Lett.* **2015**, 42, 1619–1625.
- Savastano, G.; Komjathy, A.; Verkhoglyadova, O.; Mazzoni, A.; Crespi, M.; Wei, Y.; Mannucci, A.J. Real-time detection of tsunami ionospheric disturbances with a stand-alone GNSS receiver: A preliminary feasibility demonstration. *Sci. Rep.* **2017**, 7, 1–10.
- Zhang, X.; Tang, L. Detection of ionospheric disturbances driven by the 2014 Chile tsunami using GPS total electron content in New Zealand. *J. Geophys. Res. Sp. Physics* **2015**, 120, 1–8.
- Liu, Y.; Jin, S. Ionospheric Rayleigh Wave Disturbances Following the 2018 Alaska Earthquake from GPS Observations. *Remote Sens.* **2019**, 11, 901.
- Zhang, Q.; Zhao, Q. Analysis of the data processing strategies of spherical harmonic expansion model on global ionosphere mapping for moderate solar activity. *Adv. Sp. Res.* **2019**, 63, 1214–1226.



Thank You Thank You Thank